

One-step electrodeposition synthesis and electrochemical properties of Cu_6Sn_5 alloy anodes for lithium-ion batteries

Xiao-Yong Fan · Quan-Chao Zhuang ·
Guo-Zhen Wei · Ling Huang · Quan-Feng Dong ·
Shi-Gang Sun

Received: 15 June 2008 / Accepted: 14 January 2009 / Published online: 5 February 2009
© Springer Science+Business Media B.V. 2009

Abstract Cu_6Sn_5 alloys were successfully electrodeposited on rough Cu foils and smooth Cu sheets using a facile one-step electrodeposition method, and their structural and electrochemical properties were examined by X-ray diffraction (XRD), scanning electron microscopy (SEM), galvanostatic charging/discharging testing and electrochemical impedance spectroscopy (EIS). The influence of surface morphology of the current collectors on the cycleability and the interfacial performance of the Cu_6Sn_5 alloy electrode are both discussed. The results demonstrate that the Cu_6Sn_5 alloy electrode on the rough Cu foil presented better electrochemical performance than that on the smooth Cu sheet because its rough surface could buffer the volume changes to some extent. The first discharging (lithiation) and charging (delithiation) capacities were measured at 462 and 405 mAh g^{-1} respectively with high initial coulomb efficiency of 88%, with charging capacity in the 50th cycle remaining 76% of that in the first cycle. The phase transformation during initial lithiation was detected by electrochemical impedance spectroscopy (EIS) and its trend versus electrode potential is also discussed.

Keywords Lithium-ion battery · Cu_6Sn_5 alloy ·
Rough Cu foil · Phase transformation · EIS

X.-Y. Fan
School of Materials Science and Engineering,
Chang'an University, Xi'an 710061, China
e-mail: fandajiao@yahoo.com.cn

X.-Y. Fan · Q.-C. Zhuang · G.-Z. Wei · L. Huang ·
Q.-F. Dong · S.-G. Sun (✉)
State Key Lab of Physical Chemistry of Solid Surfaces,
Department of Chemistry, College of Chemistry and Chemical
Engineering, Xiamen University, Xiamen 361005, China
e-mail: sgsun@xmu.edu.cn

1 Introduction

Lightweight and compact, lithium-ion batteries have proved to be ideal energy storage devices in appliances such as laptops, mobile phones and electric vehicles. Developing application of these devices has demanded a rise in battery energy density. However, mainstream lithium-ion batteries based on a carbon/graphite anode and a transition metal-oxide cathode are approaching their technological limit. Tin presents an attractive alternative to graphite as anode material for lithium-ion batteries due to its high gravimetric and volumetric capacities [1]. However, tin has not come to application due to its poor cycleability caused by large volume changes during lithiation/delithiation. In comparison with tin, tin-based alloys exhibit better cycleability due to inactive elements in the alloy buffer volume changes during charge/discharge cycling. Recently, tin-based alloys such as Sn–Zn [2, 3], Sn–Sb [4, 5], Sn–Co [6, 7] and Sn–Cu [8–14] have been intensively investigated and much improvement has been achieved. Among these alloys, Cu_6Sn_5 is one of the most promising anode materials because of its low price, high conductivity and good retention of capacity. Electrodeposition has been used to prepare metal and alloy materials due to its low cost and suitability for large-scale manufacture [12–14]. Although many efforts have been devoted to obtaining Cu–Sn alloys using electrodeposition in a single bath, bronzes consisting of small tin content were mainly reported. To overcome this drawback, a pulsed electrodeposition method developed by Dahn's group allows increase of the tin content in the deposits [12]. However, it is hard to accurately control the pulse parameters to obtain the expected alloy phases. Tamura et al. [13] have also fabricated Cu–Sn alloys with improved electrochemical performance by annealing the electrodeposited tin layer. Nevertheless, a thick and uniform Cu–Sn layer is

difficult to obtain through this method. Pu et al. [14] have fabricated Cu–Sn alloy electrodes with a Cu protective layer coating on the surface by electrodeposition and annealing. Although the capacity retention is high, the thickness of the Sn and Cu layer is not well controlled.

Although the relationship between morphology and electrochemical properties of alternative materials to graphite, and of graphite itself, has been under study [15], only minor studies have been devoted to the influence of the surface structure and morphology of the current collectors on the electrochemical performance of electrode materials. Recently, Fujitani et al. [16] studied the effect of the surface roughness of Cu foil, the current collector generally used for the negative electrode, on improving cycleability data. They attributed this improvement to the formation of a microcolumnar structure of the deposits, which cracks periodically in accordance with the surface profile of the Cu foil, providing space for the active materials to stretch either upwards or sideways during charging. By contrast, flat surfaces crack randomly, so that the active materials easily pulverize and delaminate from the foil. Arbizzani et al. [17] have investigated the lithiation/delithiation performance of Cu_6Sn_5 alloy electrodes using carbon paper as the current collector. The results demonstrated that good cycleability was achieved, assisted by the three-dimensional conductive matrix with micrometric, interconnected carbon fibers. Recently, Park et al. [18] have also found that a Sn-anode electroplated on the nodule-type copper substrate and annealed for 1 h at 200°C had the best performance. In addition, although the mechanism of lithiation/delithiation of Cu_6Sn_5 alloy electrodes has been extensively studied, little literature has been devoted to the interfacial performance of Cu_6Sn_5 alloy electrodes in commercial electrolytes, which is also important to improve their electrochemical performance.

In this paper, Cu_6Sn_5 alloy anodes were successfully prepared by a facile one-step electrodeposition method. The effects of surface morphology and structure of the current collector on the electrochemical performance of the Cu_6Sn_5 alloy electrode were investigated by scanning electron microscopy (SEM). Also, the interfacial performance, especially the phase transformation of the Cu_6Sn_5 alloy electrode on the rough Cu foil during lithiation, was studied by EIS for the first time in our work.

2 Experimental

2.1 Preparation of Cu_6Sn_5 alloy electrodes

Cu_6Sn_5 alloys were galvanostatically deposited on smooth Cu sheets and rough Cu foils with a current density of

Table 1 Condition of the electrodeposition bath

Reagents	Concentration (g L^{-1})
$\text{SnCl}_2 \cdot 2\text{H}_2\text{O}$	20
$\text{CuSO}_4 \cdot 5\text{H}_2\text{O}$	4
$\text{K}_2\text{P}_2\text{O}_7$	180
Addition reagent a	1
Addition reagent b	1
Addition reagent c	0.1

0.5 A dm^{-2} . The electrodeposition condition of the Cu_6Sn_5 alloys is stated in Table 1. Before electrodeposition, both of the Cu substrates were pretreated in acetone and dilute hydrochloric solution to remove the oil and oxide on the surface. After electrodeposition, the alloys were dried at 80°C for 24 h under vacuum prior to assembling them into batteries. The area density of the Cu_6Sn_5 alloys on the rough Cu foils and smooth Cu sheets were determined at $\sim 1.2 \text{ mg cm}^{-2}$ and $\sim 0.5 \text{ mg cm}^{-2}$ respectively.

2.2 Materials characterization

The morphology of all electrodeposits was analyzed by scanning electron microscopy (LEO 1530 Field Emission Scanning Electron Microscope, Oxford Instrument). The crystal structures of all deposits were examined by X-ray diffraction (XRD) measurements at room temperature using an X'pert PRO diffractometer with Cu K α radiation ($\lambda = 1.5418 \text{ \AA}$) with the collecting range of $25\text{--}90^\circ$, and analyzed using the JCPDS database.

2.3 Electrodes preparation and electrochemical characterization

Coin-type cells were assembled in an argon-filled dry glove box using the Cu_6Sn_5 alloy as the positive electrode and the Li metal as the negative electrode. The positive electrode and negative electrode were electrochemically separated by membrane (Celgard 2400). The electrolyte was 1 M LiPF_6 in a mixture of ethylene carbonate (EC) and dimethyl carbonate (DMC) (1:1 by volume, provided by Guotaihuarong, Zhangjiagang, China). The cells were galvanostatically charged and discharged at a current density of 50 mA g^{-1} over potential range $0.02\text{--}1.0 \text{ V vs. Li/Li}^+$. Electrochemical impedance spectroscopy was carried out on a PARSTAT 2263 (Princeton) using a coin-type cell over a frequency range $100 \text{ kHz to } 10 \text{ mHz}$ with a signal amplitude of 5 mV .

3 Results and discussion

3.1 The structure of as-deposited Cu_6Sn_5 alloys

Figure 1 shows the XRD patterns of the Cu–Sn alloys on the smooth Cu sheet (Fig. 1a) and rough Cu foil (Fig. 1b). Three phases coexist in both of the Cu–Sn alloys, i.e., Cu_6Sn_5 (JCPDS Card No. 03-065-2303), Sn (JCPDS Card No. 00-001-09260) and Cu (JCPDS Card No. 00-002-1225, which may be attributed to the Cu substrate). This indicates

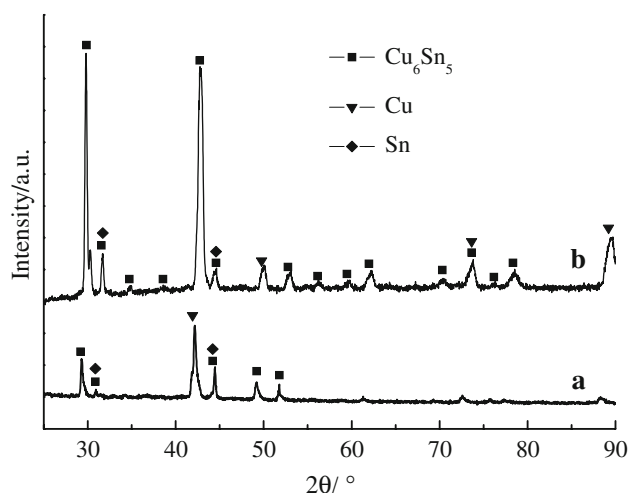
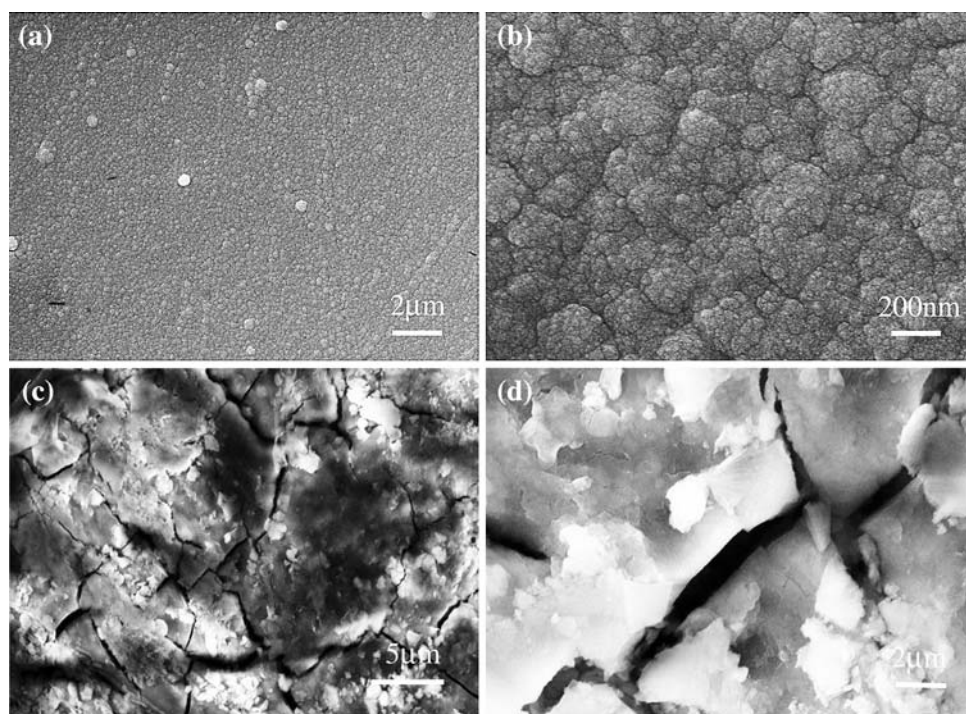


Fig. 1 XRD patterns of the Sn–Cu alloy electrodes on the smooth Cu sheet (a), and rough Cu foil (b)

Fig. 2 The SEM images of the Cu_6Sn_5 alloy electrode (a and b), and after 39 charge/discharge cycles (c, d) using the smooth Cu sheet as the current collector

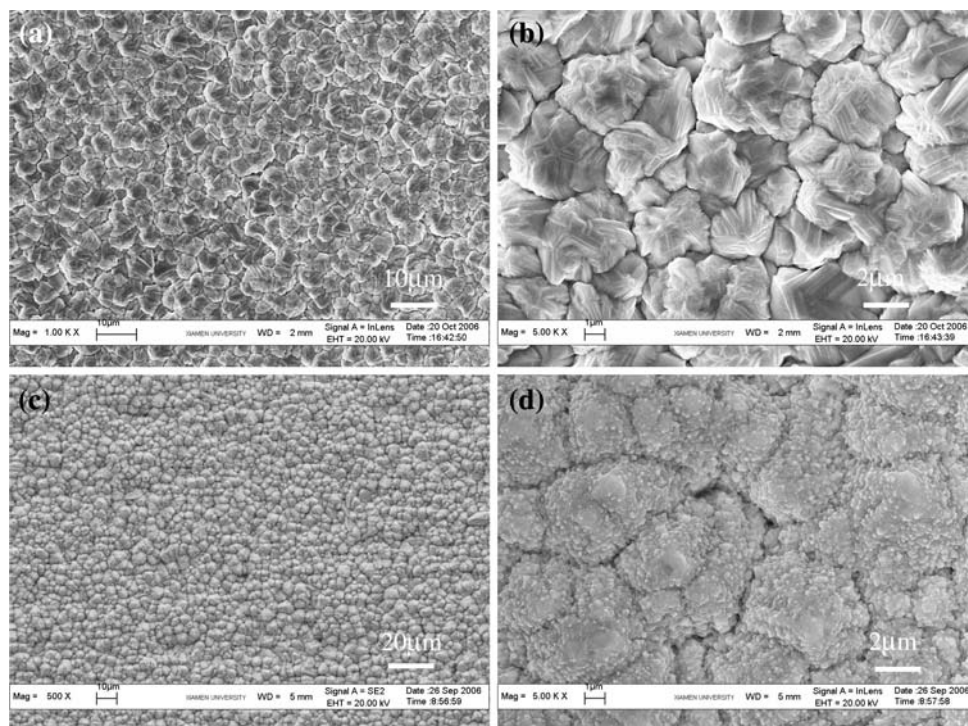


that the Cu_6Sn_5 alloy can be fabricated by the direct electrodeposition method.

3.2 The surface morphology characterization of the Cu_6Sn_5 alloy electrodes

Figure 2 shows SEM images of the Cu_6Sn_5 alloy electrodes on the smooth Cu sheet before cycling and after 39 cycles. Owing to the smooth surface's inability (Fig. 2a, b) to provide space to accommodate the volume changes during charging and discharging, serious random cracks and exfoliation appear on the electrode surface after 39 cycles (Fig. 2c, d), which is one of the main reasons for capacity failure. Figure 3 displays the SEM images of the bare rough Cu foil and the as-deposited Cu_6Sn_5 alloy on the rough Cu foil. Many small “micro-islands” and “gaps” are distributed on the surface of the rough Cu foil (see Fig. 3a, b), which improves the specific surface area as well as strengthens the adhesion between the Cu substrate and the deposits. The large specific area improves electrochemical capacity and the good adhesion guarantees high capacity retention. After depositing Cu_6Sn_5 alloy (Fig. 3c, d), the electrode surface becomes rougher with many nano-particles on the surface of each “micro-island”. After initial lithiation (Fig. 4a, b), the surface structure of the Cu_6Sn_5 alloy electrode becomes smooth with “micro-islands” and “gaps” disappearing. It is known that large volume expansion appears during initial lithiation, which causes active materials to stretch upwards and sideways, resulting in the “gaps” between the “micro-islands” filling up.

Fig. 3 SEM images of the rough Cu foil (a, b), and the Cu_6Sn_5 alloy on the rough Cu foil (c, d)



When the Cu_6Sn_5 alloy electrode undergoes one cycle (Fig. 4c, d), the surface structure is split into many “micro-islands” again, which indicates that the surface structure can expand and contract reversibly to some extent. When the Cu_6Sn_5 alloy electrode undergoes five electrochemical cycles (Fig. 4e, f) the surface structure is similar to that of the Cu_6Sn_5 alloy electrode for one cycle. However, there are no longer obvious “micro-islands” or “gaps” after 50 cycles (Fig. 4g, h). This shows that the electrode surface structure cannot contract again after many expansions and contractions. Further, there is no obvious exfoliation of active materials on the electrode surface and good electronic contact between the substrate and the Cu_6Sn_5 alloy remains: this ensures the high capacity retention discussed in the following.

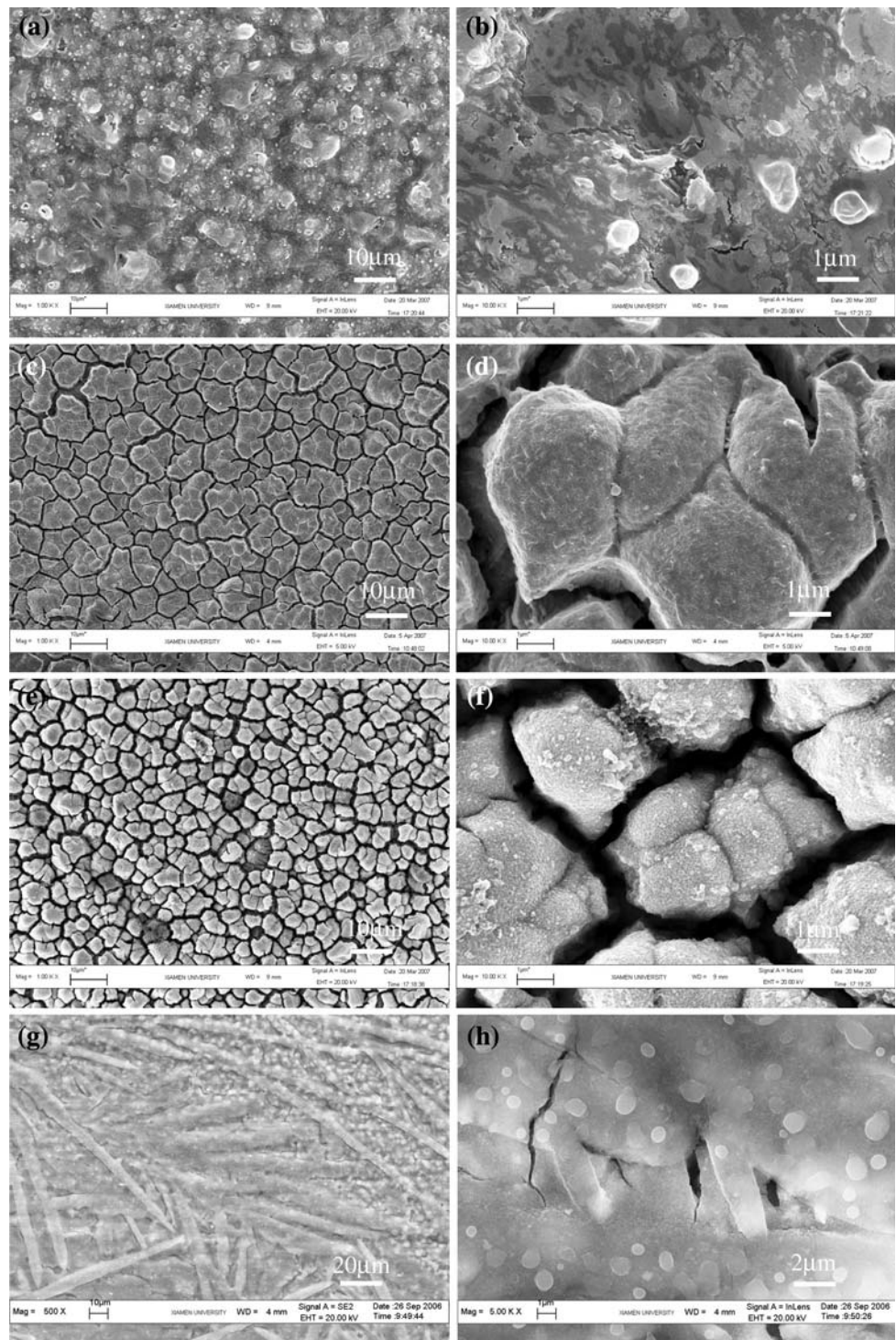
3.3 Charge and discharge characterization of the Cu_6Sn_5 alloy electrodes

The charging/discharging curves of the Cu_6Sn_5 alloy electrode on the rough Cu foil and smooth Cu sheet are respectively shown in Fig. 5a, b. Both electrodes are cycled in the potential range 0.02–1.0 V with a current density of 50 mA g^{-1} . From the first discharging curve of the electrode on the rough Cu foil (see Fig. 5a), there are two obvious plateaus at potentials of ~ 0.4 and ~ 0.1 V. According to the literature and based on our experimental data, the plateau at ~ 0.4 V represents the transformation

of Cu_6Sn_5 into $\text{Li}_x\text{Cu}_6\text{Sn}_5$ ($0 < x < 13$), which is ascribed to formation of Li_2CuSn , and the plateau at ~ 0.1 V represents the transformation of Li_2CuSn into Li_ySn ($2 < y < 4.4$) [11, 12]. The shape of the discharging potential curves and the position of potential plateaus remain similar in the initial five cycles. However, the discharging/charging potential plateaus are nearly transformed into an oblique line after 20 cycles, which indicates that the active materials are gradually transformed into another phase. From Fig. 5b it can be observed that the discharging/charging curves of the Cu_6Sn_5 alloy electrode on the smooth Cu sheet have similar shape and behavior to that of the electrode on the rough Cu foil, except that the capacity degrades more rapidly than that on the rough Cu foil.

Figure 6 displays the cycleability and coulombic efficiency curves of the Cu_6Sn_5 alloy electrodes. The first discharging and charging capacities of the Cu_6Sn_5 alloy electrode on the smooth Cu sheet are 573 and 459 mAh g^{-1} respectively which, however, degrade rapidly to 228 and 206 mAh g^{-1} respectively after 39 cycles. Also the initial discharging and charging capacities of the Cu_6Sn_5 alloy electrode on the rough Cu foil are 462 and 405 mAh g^{-1} respectively, which are lower than that of the Cu_6Sn_5 alloy electrode on the smooth Cu sheet, but they can retain 70% and 76% of the initial discharging/charging capacities after 50 electrochemical cycles. It is evident from Fig. 2 that the Cu_6Sn_5 alloy electrode on the smooth

Fig. 4 SEM images of the Cu_6Sn_5 alloy on the rough Cu foil after initial lithiation (**a, b**), initial delithiation (**c, d**), five cycles (**e, f**), and 50 cycles (**g, h**)



Cu sheet suffers serious exfoliation after repeated cycling owing to insufficient space on the surface to accommodate the volume changes: as a result the capacities decrease rapidly. In contrast, the “micro-islands” and “gaps” on the rough Cu_6Sn_5 alloy electrode can buffer the volume expansion of active materials to some extent (see Fig. 4), and, as a result, the active materials adhere strongly to the

substrate and provide good electronic contact, which is one of the main reasons for high capacity retention when compared with the Cu_6Sn_5 alloy electrode on the smooth Cu sheet. Figure 6 also gives the coulombic efficiencies of both of electrodes. The initial coulombic efficiency of the Cu_6Sn_5 alloy electrode on the rough Cu foil (88%) is higher than that on the smooth Cu sheet (80%).

Fig. 5 Charge/discharge profiles of the Cu_6Sn_5 electrode with rough Cu foil (**a**), and smooth Cu sheet (**b**), as current collector at the current density of 50 mA g^{-1} in the potential range of 0.02–1.0 V

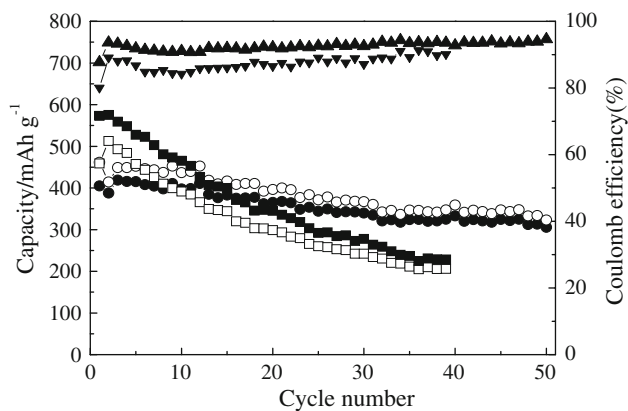
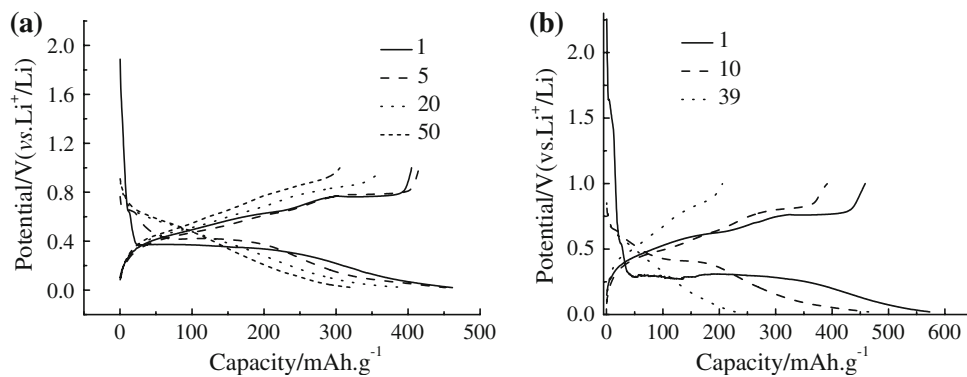


Fig. 6 Discharge (○) and charge (●) capacity of the Cu_6Sn_5 electrode on the rough Cu foil, and discharge (■) and charge (□) capacity of the Cu_6Sn_5 electrode on the smooth Cu sheet, and coulomb efficiency of the Cu_6Sn_5 electrode on the rough Cu foil (▲) and smooth Cu sheet (▼)

3.4 Electrochemical impedance spectroscopy characterization of the Cu_6Sn_5 alloy electrode on the rough Cu foil

Electrochemical impedance spectroscopy (EIS) is one of the most promising tools for modelling and diagnosis of interfacial reactions. It can even analyze the sources of battery impedance and identify battery failure using an appropriate equivalent-circuit model. The shape and value of the resistance in the impedance spectra were found to be strongly affected by solvents, particle size, thickness of electrodes and stack pressure.

To study the interfacial performance of the Cu_6Sn_5 alloy electrode on the rough Cu foil, the electrochemical impedance spectra (Nyquist representation) were examined and are shown in Fig. 7. The graph obtained before lithiation (Fig. 7a) shows a high frequency (HF) arc and a slightly inclined line in the low frequency (LF) region, which represents the blocking character of the non-lithiated electrode at the equilibrium electrode potential. When the electrode potential is negatively polarized to the lithiated

region (Fig. 7b–d), the graphs show a similar high frequency arc to that of the equilibrium electrode potential, and another new arc appearing in the medium frequency (MF) region.

In general, the HF arc is attributed to the impedance of the solid electrolyte interphase (SEI) film on the electrode surface. However, for our studied system, the HF arc may be largely attributed to contact impedance and a minor contribution from SEI film impedance because there is no obvious change detected during the entire negatively polarized process, which is the most important character of SEI impedance [19]. When the potential of the Cu_6Sn_5 alloy electrode is negatively polarized to 0.45 V (see Fig. 7b), a new arc appears in the medium frequency region, which can be attributed to the impedance of charge transfer during lithiation. When the electrode potential is negatively polarized to 0.375 V, the diameter of the MF arc begins to become smaller, indicating insertion of a large amount of lithium ions. This phenomenon can be proved in the initial discharging curve as illustrated in Fig. 5a, in which the main lithiation (discharging) process occurs at ~ 0.4 V. Meanwhile, the inclined straight line in the low frequency region is transformed into a large arc in the potential range 0.375–0.35 V, and, as a result, three impedance arcs appear in the Nyquist plots. Three impedance arcs can also be observed in the Nyquist plots of LiCoO_2 , LiMn_2O_4 and other electrode materials during lithiation or delithiation. Zhuang et al. [20] attributed this phenomenon to the appearance of electronic impedance because their systems were semiconductors. However, for our system, this new arc cannot be attributed to electronic impedance because the Cu_6Sn_5 alloy electrode has high electronic conductivity.

It is evident from Fig. 5a that there appears one phase transformation process from Cu_6Sn_5 to $\text{Li}_x\text{Cu}_6\text{Sn}_5$ ($0 < x < 13$) at ~ 0.4 V with large volume expansion. Owing to large differences between the physical/chemical properties of the Cu_6Sn_5 phase and that of the $\text{Li}_x\text{Cu}_6\text{Sn}_5$ ($0 < x < 13$) phase, two independent time constants for

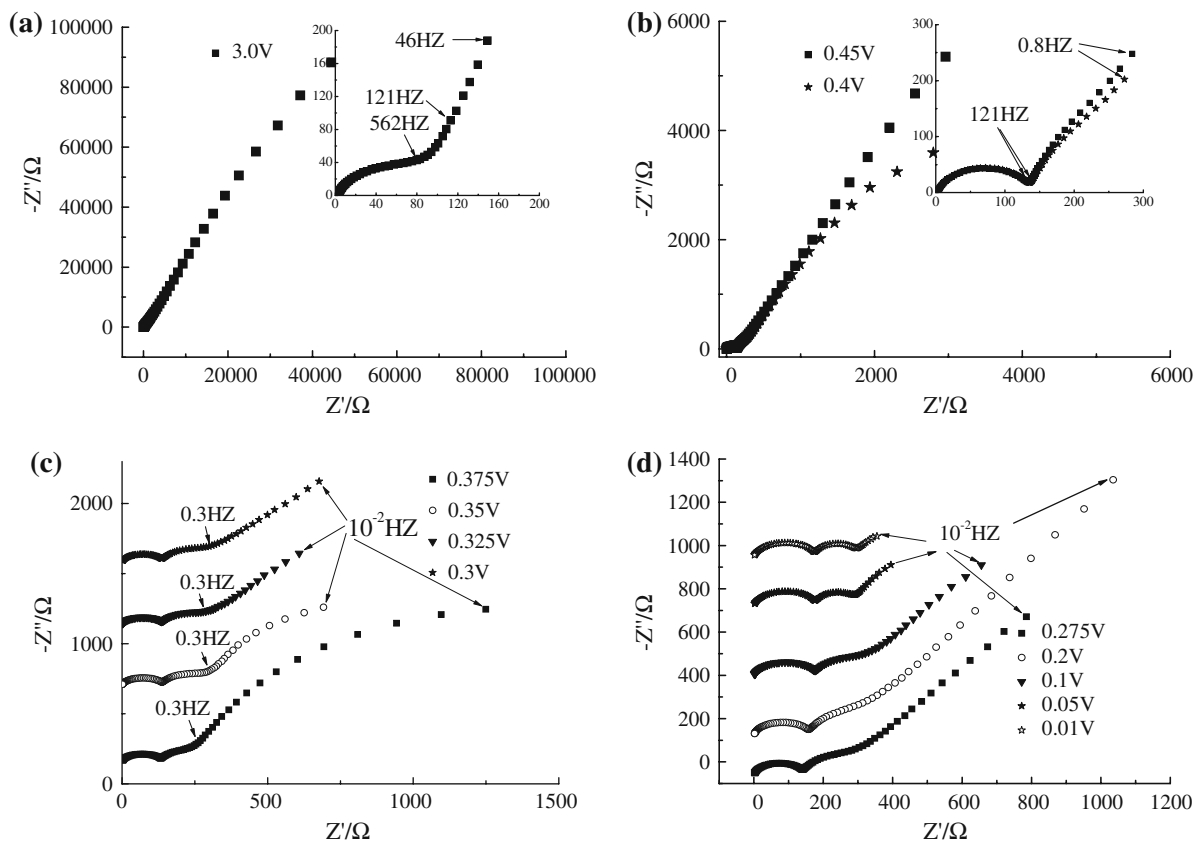


Fig. 7 Evolution of impedance spectra (Nyquist representation) of the Cu_6Sn_5 alloy electrode on the rough Cu foil during the first lithiation

lithium-ion transference in the two phases appear and, as a result, a new arc is detected in the low frequency region in the Nyquist plots.

Based on the above analysis and according to the literature [21–24], this new arc can be attributed to phase transformation from the Cu_6Sn_5 phase to the $\text{Li}_x\text{Cu}_6\text{Sn}_5$ ($0 < x < 13$) phase. However, for LiCoO_2 , LiMn_2O_4 and other electrode materials, although there is also phase transformation during lithiation or delithiation, the physical/chemical properties of the co-existing phases are similar, so the impedance arc associated with phase transformation cannot be observed in the Nyquist plots. It is interesting that the LF arc transforms into one inclined straight line again as the electrode potential is negatively polarized below 0.325 V (see Fig. 7c). It is noted from Fig. 5a that the phase transformation becomes less obvious when the potential is below 0.325 V, so the LF arc transforms into one inclined straight line. However, when the potential is decreased to 0.05 V, the LF arc appears again. From Fig. 5a there appears another phase transformation process from Li_2CuSn into Li_ySn ($2 < y < 4.4$) in this potential region, which causes a LF arc to again appear in the Nyquist plots.

4 Conclusions

Cu_6Sn_5 alloy electrodes were successfully fabricated by electrodeposition using rough Cu foils and smooth Cu sheets as the current collectors. Their structure, morphology and electrochemical performance were examined by XRD, SEM, galvanostatic charging/discharging testing and electrochemical impedance spectroscopy. The as-deposited Cu–Sn alloys were determined as the intermetallic composite of Cu_6Sn_5 with impure phases of Sn and Cu using XRD analysis. The rough surface of the Cu_6Sn_5 alloy electrode was shown by SEM to be able to accommodate the volume changes during lithiation/delithiation, and provide good electronic contact between the substrate and the active materials, ultimately improving capacity retention compared with that of the Cu_6Sn_5 alloy electrode on the smooth Cu sheet. The interfacial performance of the Cu_6Sn_5 alloy electrode on the rough Cu foil was analyzed by electrochemical impedance spectroscopy. A low frequency arc demonstrating phase transformation was detected in the Nyquist plots during initial lithiation and its evolution was shown to be consistent with that of charging/discharging curves.

Acknowledgements This work was financially supported by the Major State Basic Research Development “973” Program of China (2009CB220102) and National Natural Science Foundation of China (No. 20773102).

References

1. Idota Y, Kubota T, Matasufuji A, Maekawa Y, Miyasaka T (1997) *Science* 276:1395
2. Wang LB, Kitamura S, Sonoda T, Obata K, Tanase S, Sakaia T (2003) *J Electrochem Soc* 150:A1346
3. Wang LB, Kitamura S, Obata K et al (2005) *J Power Sources* 141:286
4. Shi LH, Li H, Wang ZX, Huang XJ, Chen LQ (2001) *J Mater Chem* 11:1502
5. Li H, Shi LH, Lu W, Huang XJ, Chen LQ (2001) *J Electrochem Soc* 148:A915
6. Tamura N, Kato Y, Mikami A, Kamino M, Matsuta S, Fujitani S (2006) *J Electrochem Soc* 153:A1626
7. Zhang JJ, Xia YY (2006) *J Electrochem Soc* 153:A1466
8. Kepler KD, Vaughey JT, Thackray MM (1999) *J Power Sources* 81–82:383
9. Kepler KD, Vaughey JT, Thackray MM (1999) *Electrochem Solid State Lett* 2:307
10. Thackray MM, Vaughey JT, Johnson CS, Kropf AJ, Benedek R, Fransson LML, Edstrom K (2003) *J Power Sources* 113:123
11. Larcher D, Beaulieu LY, Macneil DD, Dahn JR (2000) *J Electrochem Soc* 147:1658
12. Beattie SD, Dahn JR (2003) *J Electrochem Soc* 150:A894
13. Tamura N, Ohshita R, Fujimoto M, Fujitani S, Kamino M, Yonezu I (2002) *J Power Sources* 107:48
14. Pu WH, He XM, Ren JG, Wan CR, Jiang CY (2005) *Electrochim Acta* 50:4140
15. Wolfenstine J, Campos S, Foster D, Read J, Behl WK (2002) *J Power Sources* 109:230
16. Tamura N, Ohshita R, Fujimoto M, Kamino M, Fujitani S (2003) *J Electrochem Soc* 150:A679
17. Arbizzani C, Lazzari M, Mastragostino M (2005) *J Electrochem Soc* 152:A289
18. Park JW, Rajendran S, Kwon HS (2006) *J Power Sources* 159:1409
19. Holzappel M, Marinent A, Allion F, Lee BG, Yazami R, Montella C (2003) *J Electroanal Chem* 546:41
20. Zhuang QC, Xu JM, Fan XY, Dong QF, Jiang YX, Huang L, Sun SG (2007) *Chin Sci Bull* 52:147
21. Barsoukov E, Kim JH, Kim DH, Hwang KS, Yoon CO, Lee H (2000) *J New Mater Electrochem Syst* 3:301
22. Hong J, Wang CS, Kasavajjula U (2006) *J Power Sources* 162:1289
23. Levi MD, Aurbach D (2007) *J Solid State Electrochem* 11:1031
24. Bisquert J, Randriamahazaka H, Garcia-Belmonte G (2005) *Electrochim Acta* 51:627